

Spatiotemporal Patterns of Granule Cell Activity Revealed by a Large-Scale, Biologically Realistic Model of the Hippocampal Dentate Gyrus



Gene J. Yu, Phillip J. Hendrickson, Dong Song, and Theodore W. Berger

Abstract Interest in the hippocampus has generated vast amounts of experimental data describing hippocampal properties, including anatomical, morphological, biophysical, and synaptic transmission levels of analysis. However, this wealth of structural and functional detail has not guaranteed insight into higher levels of system operation.

In this chapter, we propose a computational framework that can integrate the available, quantitative information at various levels of organization to construct a three-dimensional, large-scale, biologically realistic, spiking neuronal network model with the goal of representing all major neurons and neuron types, and the synaptic connectivity, found in the rat hippocampus. In this approach, detailed neuron models are constructed using a multi-compartment approach.

Simulations were performed to investigate the role of network architecture on the spatiotemporal patterns of activity generated by the dentate gyrus. The results show that the topographical projection of axons between the entorhinal cortex and the dentate granule cells organizes the postsynaptic population into subgroups of neurons that exhibit correlated firing expressed as spatiotemporal clusters of firing. These clusters may represent a potential “intermediate” level of hippocampal function. Furthermore, the effects of inhibitory and excitatory circuits, and their interactions, on the population granule cell response were explored using dentate basket cells and hilar mossy cells.

G. J. Yu (✉) · P. J. Hendrickson · D. Song · T. W. Berger

Department of Biomedical Engineering, Center for Neural Engineering, Viterbi School of Engineering, University of Southern California, Los Angeles, CA, USA

e-mail: geneyu@usc.edu; phendric@usc.edu; dsong@usc.edu; berger@usc.edu

© Springer Nature Switzerland AG 2018

V. Cutsuridis et al. (eds.), *Hippocampal Microcircuits*, Springer Series

in Computational Neuroscience, https://doi.org/10.1007/978-3-319-99103-0_12

473

Overview

Comprehensive Computational Framework for Neural Systems

Possibly more than any other brain area, interest in the hippocampus has generated vast amounts of experimental data through the efforts of the neuroscience community. This has led to the accumulation of large amounts of quantitative information describing the properties of the hippocampus, including anatomical, morphological, biophysical, biochemical, and synaptic transmission levels of analysis. As with other brain areas, however, this wealth of structural and functional detail has not guaranteed insight into higher levels of system operation. The field continues, and rightfully so, to struggle to understand how all of the cellular and network properties of the hippocampus dynamically interact to produce the global functional properties of the larger system.

Multiple theories and hypotheses have been put forward to contextualize and interpret subsets of the huge amount of hippocampal data. These works have attempted to provide possible explanations for various behavioral and cognitive functions believed to be subserved by the hippocampus (Marr 1971; McNaughton and Morris 1987; Levy 1989; Treves and Rolls 1994; McClelland et al. 1995; Hasselmo 2005; Solstad et al. 2006; Myers and Scharfman 2011). Although these studies are highly admirable and have helped guide the field in its thinking about the cellular and network bases of hippocampal memory, they are limited by the narrow or partial scope of the quantitative experimental data on which they are based and by the multiple levels of neural organization that various models and theories must “reach over” to account for system/behavioral phenomena. There remain few computational frameworks (see Morgan and Soltesz 2010) that integrate at least a significant portion of the quantitative cellular and anatomical data of the hippocampus for its multiple subfields. As a consequence, there are no models to date that successfully integrate such data and extend those “lower-level” properties to putative explanations of “higher-level” function, be it at the system level or the cognitive and behavioral levels.

Hippocampal Architectural Constraints on Network Function

If there is any one brain structure that provides an opportunity for understanding integration from molecular to system neural function, it is the hippocampus. One basis for this argument has already been mentioned, namely, the large body of quantitative information already collected about its molecular, cellular, and network structure and function. The second basis is the nature and relative simplicity of the structural organization of the hippocampus.

There is a highly well-defined organization to the hippocampal formation consisting of a predominantly feedforward architecture wherein activity is propagated

from entorhinal cortex to the dentate gyrus, to the CA3/4 pyramidal zones, and finally to the CA1/2 pyramidal regions (Andersen et al. 1971; Swanson et al. 1978). The projections between each of the subfields exhibit unique organizational principles (e.g., targets and topography) (Swanson et al. 1978; Ishizuka et al. 1990; Freund and Buzsáki 1996; Dolorfo and Amaral 1998). These studies reveal a topographic projection between neural populations in that they are incomplete (in the sense that any one neuron within a subfield does not project to all neurons in the next subfield) and nonrandom nature of hippocampal connectivity. The topography describes the ordered structural connectivity of a neural system which organizes individual neurons into collections of neurons and offers a bridge between lower-level cellular dynamics and higher-level population dynamics.

General Framework of the Model

We are proposing a computational framework that is able to integrate the majority of available, quantitative structural and functional information at various levels of organization to generate a large-scale, biologically realistic, neuronal network model with the goal of representing all of the major neurons and neuron types, and the synaptic connectivity, found in one hemisphere of the rat hippocampus. In this approach, detailed neuron models are constructed using a multi-compartment approach (on the order of hundreds of compartments per neuron) which are then geometrically arranged based on anatomical data to encompass the entire longitudinal extent of the hippocampus and finally synaptically connected using the topographical constraints describing the region.

Using this framework, a series of simulations were performed which primarily explored the role of network architecture on the spatiotemporal patterns of activity generated by populations of granule cells in the dentate gyrus. The simulations involved pulse (all-or-none, spike-like) inputs from layer II cells of the entorhinal cortex and the spike-like granule cell and basket cell outputs from the dentate gyrus, with AMPA receptor channel-mediated excitatory synapses of granule cells and GABA_A receptor channel-mediated inhibitory synapses of basket cells. The simulations in this chapter show specifically that the *topographical projection* of axons between the entorhinal cortex and the dentate granule cell regions of the hippocampal formation organizes the postsynaptic population into subgroups of neurons that exhibit correlated firing expressed as *spatiotemporal clusters* of firing. These findings strongly suggest that topography may act as a spatial filter whose functional characteristics are dependent on the three-dimensional properties of that topography. During this investigation, the effects of inhibitory and excitatory circuits, and their interactions, on the population granule cell response also were systematically explored by including study of feedforward and feedback inhibition and study of the hierarchical regulation of lower-level excitatory and inhibitory circuitry by dentate hilar mossy cells.

“Intermediate” Levels of System Function

One of the fundamental issues that has arisen in using our multi-level model of the hippocampus is that there is a need to identify what might be termed “intermediate” levels of hippocampal function. There are generally well-understood interpretations of “synaptic function” (presynaptic release, postsynaptic current and/or potential, etc.) and “cellular function” (metabolism, action potential generation, etc.). Although there are multiple possible definitions for each level of functionality, there is general agreement on what are the small number of possibilities in each case. But once “molecular,” “synaptic,” and “cellular functions” are accounted for, what is the definition of “multicellular” or “system” function, upon which there is generally little if any universal agreement? Even more difficult to address is the identification of levels of functions that lie between “cellular” or “multicellular” and behavioral or cognitive functions. Behavioral and inferred cognitive functions for the hippocampus have a theoretically rich and experimentally broad history (O’Keefe and Nadel 1978; Berger et al. 1986; Squire 1986; Berger and Bassett 1992; Cohen and Eichenbaum 1993; Nadel and Moscovitch 1997; Aggleton and Brown 1999). How hippocampal cognitive and behavioral functions derive from cellular and molecular dynamics remains a mystery.

For insights to be reached on this issue, we must identify levels of system or subsystem function that lie between the cellular and the behavioral. One of the main objectives in developing the large-scale model of the hippocampus described here was so that it would be possible to “observe” simulated spiking activity of large numbers of neurons simultaneously – the activity of many more neurons than had ever been observed previously, either computationally or experimentally. If there were regularities in granule cell firing that became apparent beyond the level of tens of neurons, i.e., beyond the levels typically used in previous studies identifying behavioral or cognitive population “correlates” of hippocampal cell activity (Berger et al. 1983, 2011; Berger and Weisz 1987; Eichenbaum et al. 1989; Hampson et al. 1999; Krupic et al. 2012; MacKenzie et al. 2014), such “regularities” in population firing of hippocampal neurons would indicate the existence of some kind of higher-level “structure” in the organization of the hippocampal system. The computational studies reviewed here have revealed one such an organizational structure: the “clusters” of granule cell firing revealed by the present analyses indicate cyclical, correlated levels of excitability distributed both in space and time throughout the rostral-caudal extent of the hippocampus in response to low levels of random entorhinal cortical activity. Because such correlated, clustering of granule cell firing is expressed to a low level of relatively even entorhinal input and does not require a radically, strong, and/or rhythmic bursting from entorhinal cortex, we believe the granule cell clusters represent a preferential space-time filtering by the dentate gyrus that constitutes a first-order level of processing by the multiple stages of hippocampal circuitry.

The Model

Though much data on the hippocampus exists, the search, quantification, and implementation of these data into a comprehensive model is problematic, considering the large variety of techniques that can be applied to characterize any particular hippocampal feature and the number of features that require investigation. Below, we review the experimental work that has been incorporated into this version of the model and the methods we used to extract and implement the results of those studies.

Anatomical Boundaries

Anatomical Description of the Hippocampus and Dentate Gyrus

The three-dimensional structure of the hippocampus resembles a curved cylinder (see Fig. 1) with a single homogeneous granule cell layer and a pyramidal cell layer that traditionally has been divided into four subsections (Lorente de N6 1934; Ramón y Cajal 1968). A cross section of the hippocampus can reveal its principal internal structure in the form of two interlocking C-shapes. One of the structures is known as the dentate gyrus, and the other is known as the cornus ammonis (CA) which is commonly divided into four main subfields, the CA3/4 and the CA1/2.

The dentate gyrus is commonly divided into two blades, the upper and lower half of its C-shape. The suprapyramidal blade, also known as the enclosed or dorsal

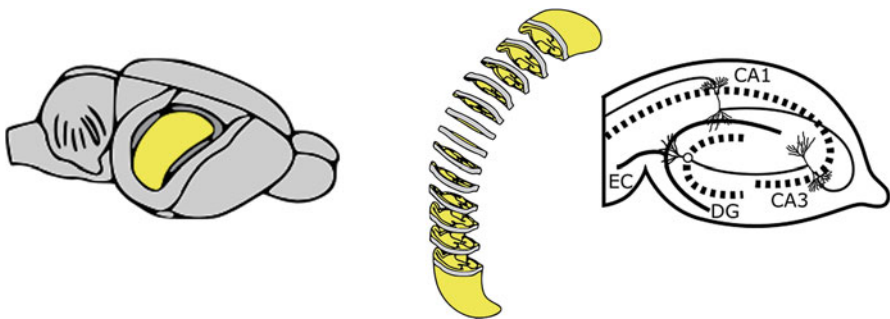


Fig. 1 Schematic representation of the rat hippocampus. (Left) Location of the hippocampus (yellow) relative to the rest of the rat brain (neocortex removed). (Middle) Depiction of how transverse slices typically are obtained relative to the septo-temporal axis of the hippocampus. (Right) The classical trisynaptic circuit of the hippocampus where the entorhinal cortex (EC) projects its inputs to the dentate gyrus (DG), the dentate projects to the CA3/4 regions, the CA3/4 projects to the CA1/2 regions, and the CA1 provides the output of the hippocampus to other cortical structures. Not shown here are entorhinal projections to the distal dendrites of CA3 (from layer II) and to the distal dendrites of CA1 (from layer III)

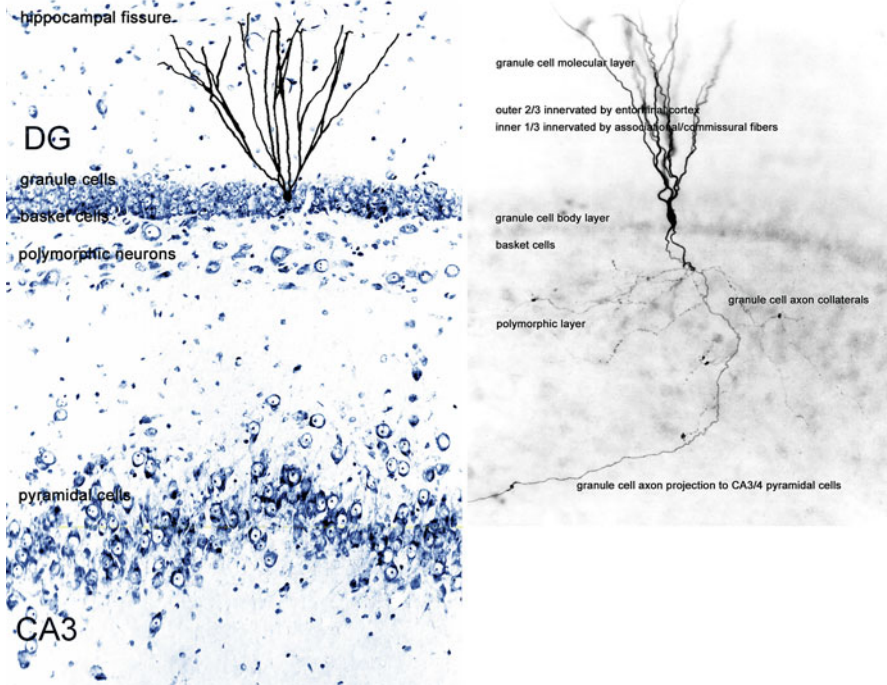


Fig. 2 Division of the dentate gyrus into the molecular, granule cell, and polymorphic layers. The molecular layer contains the dendrites of the granule cells. The densely packed cell bodies of the granule cells form the granule cell layer. The polymorphic layer is comprised of inhibitory and excitatory interneurons. Granule cell axons collateralize within the polymorphic layer to provide input to the interneurons. Granule cells also send axons through the polymorphic layer to synapse with CA3/4 pyramidal cells

blade, refers to the half of the dentate that is encapsulated by the CA regions. The remaining half is labeled the infrapyramidal blade, also known as the exposed or ventral blade, and the crest refers to the region where the infrapyramidal and suprapyramidal blades join. Furthermore, the dentate gyrus is divided into three layers. The outermost layer is the molecular layer, the middle layer is the granule cell layer, and the final layer is the hilus or the polymorphic layer (see Fig. 2).

The entorhinal cortex, which lies outside the hippocampus (but is formally defined as part of the hippocampal formation), contributes significantly to the input of the hippocampus. Layer II cells of the entorhinal cortex send axons to the outer two-thirds of the molecular layer of the dentate gyrus and synapse along the infra- and suprapyramidal blades as well as extend into and form synapses within the CA3 region (Hjorth-Simonsen and Jeune 1972; Yeckel and Berger 1990; Witter 2007). Layer III cells of the entorhinal project monosynaptically to the CA1/2 pyramidal cells (Yeckel and Berger 1995).

Formation of Anatomical Maps and Distribution of Neurons

Swanson et al. (1978) had developed a method to “unfold” the hippocampus to create two-dimensional, flattened representations of its various subfields (this flattened representation can extend to the entorhinal cortex as well) that still preserves well most of the relative anatomical geometry that exists in the original three-dimensional structure. Much of the data involving topography and the distributions of cellular populations is presented using such two-dimensional maps or, in some cases, along a one-dimensional axis. The axes describing the flattened maps can be used to easily project such two-dimensional data onto a proper three-dimensional hippocampal structure.

The work of Gaarskjaer (1978) was used in the model to create a more detailed anatomical map of the dentate gyrus due to its inclusion of both length measurements and granule cell body density measurements along the extents of both the suprapyramidal and infrapyramidal blades of the dentate gyrus. The basket cell distribution within the dentate has been less completely investigated, but ratios of granule cells and interneurons have been reported with septo-temporal and infra- and suprapyramidal differences. The granule cell/basket cell ratio in the suprapyramidal blade is approximately 100:1 at the septal end and approximately 150:1 at the temporal end, while the ratio in the infrapyramidal blade is 180:1 septally and 300:1 temporally (Seress and Pokorny 1981). The ratios were interpolated to provide a complete distribution of basket cell densities along the dentate gyrus. Buckmaster and Jongen-Rêlo (1999) reported the longitudinal distribution of mossy cells with the temporal pole having a density approximately ten times greater than that of the septal pole. The total number of the relevant neurons that are in the entorhinal-dentate system of the rat is listed in Table 1.

Multi-compartmental Neuron Models

The three main dentate neuron types that were included in the model were the granule cells, basket cells, and mossy cells. Granule cells are the principal neurons of the dentate gyrus and are situated with their somata in the granule cell layer. Their

Table 1 Cell numbers in the large-scale model

	Cell number
Lateral entorhinal cortex cells ^a	46,000
Medial entorhinal cortex cells ^a	66,000
Granule cells ^a	1,200,000
Basket cells ^b	4500
Mossy cells ^c	30,000

^aMulders et al. (1997); ^bBuckmaster and Dudek (1997); ^cBuckmaster and Jongen-Rêlo (1999)

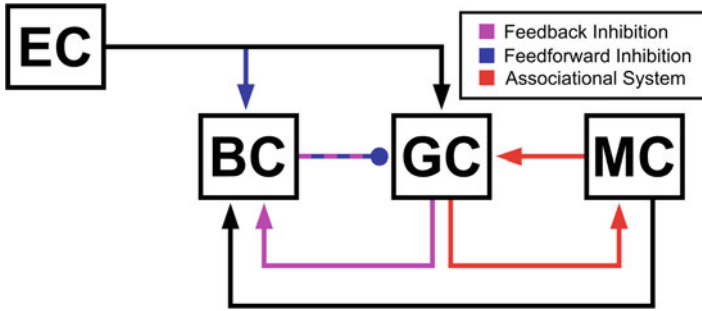


Fig. 3 Schematic of the neural circuits in the dentate gyrus model. The feedback inhibition circuit is formed by granule and basket cells. Feedforward inhibition is achieved by the entorhinal activation of basket cells. Mossy cells form the associational system and provide excitatory feedback to granule cells. Mossy cells also disynaptically inhibit granule cells by activating basket cells

apical dendrites extend into and span the molecular layer. Granule cells receive the majority of the entorhinal inputs which are excitatory. Their axons, while arborizing within the hilus, project a single primary axon, known as the mossy fiber, to cells in the CA3/4 regions.

Basket cells are interneurons within the granule cell layer that provide inhibitory input to granule cells (Gamrani et al. 1986). Many basket cells have apical dendrites that extend into the molecular layer from which they receive excitatory input from the entorhinal cortex and basal dendrites that arborize within the hilus from which they receive excitatory input from granule cells (Seress and Pokorny 1978; Ribak and Seress 1983; Zipp et al. 1989; Ribak et al. 1990; Acsády et al. 2000). Basket cell axons collateralize extensively in the granule cell layer and the innermost regions of the molecular layer where they form GABAergic synapses with granule cells, primarily on their cell bodies and the initial segments of their axons (Seress and Ribak 1983). Thus, synaptic arrangements exist that provide the basis for both feedforward and feedback inhibition (Fig. 3).

Mossy cells are hilar interneurons that contribute to the associational-commissural fibers that arise from both the ipsilateral and contralateral hippocampus (Zimmer 1971; Gottlieb and Cowan 1973; Berger et al. 1981). The dendrites of mossy cells are restricted to the hilus, but their axons collateralize extensively within the inner third of the molecular layer (Buckmaster et al. 1996; Ribak and Shapiro 2007). Mossy cells primarily serve an excitatory role by directly activating granule cells via glutamatergic synapses (Buckmaster et al. 1992; Soriano and Frotscher 1994; Ribak and Shapiro 2007). However, associational-commissural inputs have also been shown to activate inhibitory circuits within the dentate gyrus (Douglas et al. 1983; Scharfman et al. 1990; Scharfman 1995). These data indicate that mossy cells participate in both an excitatory and inhibitory capacity by monosynaptically exciting granule cells and disynaptically inhibiting granule cells

via other interneurons. In the present model, basket cells receive input from the mossy cells to provide the disynaptic inhibitory effect mediated by the mossy cells (Fig. 3).

Generation of Dendritic Morphologies

Neurons are commonly classified, in part, based on stereotypical morphological features that describe the branching of their dendrites. The diversity of morphological types has led many neuroscientists to investigate the functional role of different branching characteristics. The dendritic morphology of neurons has been shown to greatly influence several factors during input processing such as the propagation and attenuation of postsynaptic potentials and the linear or nonlinear integration of multiple inputs (Krueppel et al. 2011). Given this morphological diversity and its functional importance, the database NeuroMorpho.Org was used to obtain three-dimensional reconstructions of granule cell morphologies which were then used to generate the distributions of the relevant parameters using L-Measure (Rihn and Claiborne 1990; Ascoli et al. 2007; Scorcioni et al. 2008). The parameters were used by a software tool called L-NEURON to generate unique dendritic morphologies for each granule cell in the network (Ascoli and Krichmar 2000; see Hendrickson et al. 2015). The parameters provide the geometrical points at which a bifurcation can occur, the number of branches, their angles, etc. (see Table 2).

The dendritic morphology of basket cells and mossy cells varies as a function of cell location and the shape of the curvature of the hippocampus at that location. Due to the limited sample size of reconstructions, proper morphologies were not considered for these cell types. Due to the lack of information and to decrease

Table 2 Morphological parameters for granule cells

	Distribution	Mean/min	Std. dev./max
Soma diameter	Gaussian	9.0	2.0
Number of stems	Uniform	2	4
Stem initial diameter	Gaussian	1.51	0.39
Branching diameter	Gaussian	0.49	0.28
IBF branch length	Gaussian	10.7	8.4
Term. branch length	Gaussian	10.7	8.4
Daughter ratio	Uniform	1	2
Taper ratio	Gaussian	0.10	0.08
Rall power	Constant	1.5	–
Bifurcation amplitude	Gaussian	42	13
Tree elev. (narrow)	Gaussian	10	2
Tree elev. (medium)	Gaussian	42	2
Tree elev. (wide)	Gaussian	75	2

the computational load of the simulations, basket and mossy cells for this level of analysis were represented using a single somatic compartment.

Specification of Passive and Active Properties

The specification of morphology accounts for some of the passive propagation of electrical activity, i.e., the electrotonic response, but to create a complete model of the dendritic processing of granule cells, the parameters for passive properties needed to be augmented by active dendritic properties due to voltage-dependent channels also found in the dendritic regions (Krueppel et al. 2011).

The discretization of dendritic morphologies into compartments, the embedding of passive and active mechanisms into the compartments, and the simulation of the resulting model was performed using the NEURON simulation environment v7.3 and scripted using Python v2.8 (Carnevale and Hines 2006; Oliphant 2007; Hines et al. 2009). The passive and active properties can be set to match experimental data (see Fig. 4), much of which has been pioneered by previous groups. The works of these groups are the basis of our current neuron models (Yuen and Durand 1991; Aradi and Holmes 1999; Aradi and Soltesz 2002; Santhakumar et al. 2005). The active and passive properties used are summarized in Table 3. The resulting heterogeneous distribution of ion channel densities and the similarly heterogeneous nature of the morphologies then were able to closely approximate the electrophysiological responses of granule cells.

Topographic Connectivity

With the anatomical map and distribution of neurons within the map defined, the next step in completing the large-scale neural network was to connect the neuron models to each other. The connectivity methods used in this work are largely derived from the work of Patton and McNaughton (1995), who compiled an extensive amount of information concerning the connectivity of the dentate gyrus and described a method of distance-based probabilistic connectivity.

The present large-scale model makes a critical assumption about the function of axons in that it assumes that an axon acts merely as a propagator of action potentials from generation near the soma to the end of the terminal. Though studies exist that catalogue the role of axons in modulating synaptic transmission, the present model did not explicitly model axon morphologies and compartments. Rather, axons were functionally represented by incorporating the delay associated with the propagation of the action potential from the soma to the corresponding presynaptic terminal. This was calculated using the physical distance between the soma and the synapse and reported action potential propagation velocities.

Connectivity in the model was represented using probability distributions that were constrained by experimental data. The main concerns were, given the origin

Table 3 Distribution of passive and active properties in the neuron models

Mechanism	Granule cells		GCL	Inner third	Middle third	Outer third	Basket cells		Mossy cells	
	Soma						Soma		Soma	
C_m ($\mu\text{m}/\text{cm}^2$)	9.8		9.8	15.68	15.68	15.68	1.4		0.6	
R_a ($\Omega\text{-cm}$)	210		210	210	210	210	100		100	
^a Sodium (S/cm^2)	0.84		0.126	0.091	0.056	–	0.12		0.12	
^a Slow delayed rectifier K^+ (S/cm^2)	6e-3		6e-3	6e-3	6e-3	8e-3	–		–	
^a Fast delayed rectifier K^+ (S/cm^2)	0.036		9e-3	9e-3	2.25e-3	2.25e-3	0.013		5e-4	
^b A-type K^+ (S/cm^2)	0.108		–	–	–	–	1.5e-4		1e-5	
^c L-type Ca^{2+} (S/cm^2)	2.5e-3		7.5e-3	7.5e-3	5e-4	–	5.0e-3		6e-4	
^c N-type Ca^{2+} (S/cm^2)	7.35e-4		2.2e-3	7.35e-4	7.35e-4	7.35e-4	8.0e-4		8e-5	
^c T-type Ca^{2+} (S/cm^2)	7.4e-5		7.5e-5	2.5e-4	5e-4	1.0e-3	–		–	
^a Ca-dependent K^+ (S/cm^2)	1e-3		4e-4	2e-4	–	–	2.0e-6		0.016	
^d Ca- and V-dependent K^+ (S/cm^2)	1.2e-4		1.2e-4	2e-4	4.8e-4	4.8e-4	2.0e-4		0.0165	
^a Leak (S/cm^2)	2.9e-4		2.9e-4	4.6e-4	4.6e-4	4.6e-4	1.8e-3		1.1e-5	
^c Tau for decay of intracell. Ca^{2+} (ms)	10		10	10	10	10	10		10	
^c Steady-state intracell. Ca^{2+} (mM)	5.0e-6		5.0e-6	5.0e-6	5.0e-6	5.0e-6	5.0e-6		5.0e-6	

The equations describing the channel dynamics were originally published in the following works: ^aYuen and Durand (1991); ^bWarman et al. (1994); ^cJaffe et al. (1994); and ^dDe Schutter and Bower (1994). Reproduced from Hendrickson et al. 2016 with permission.

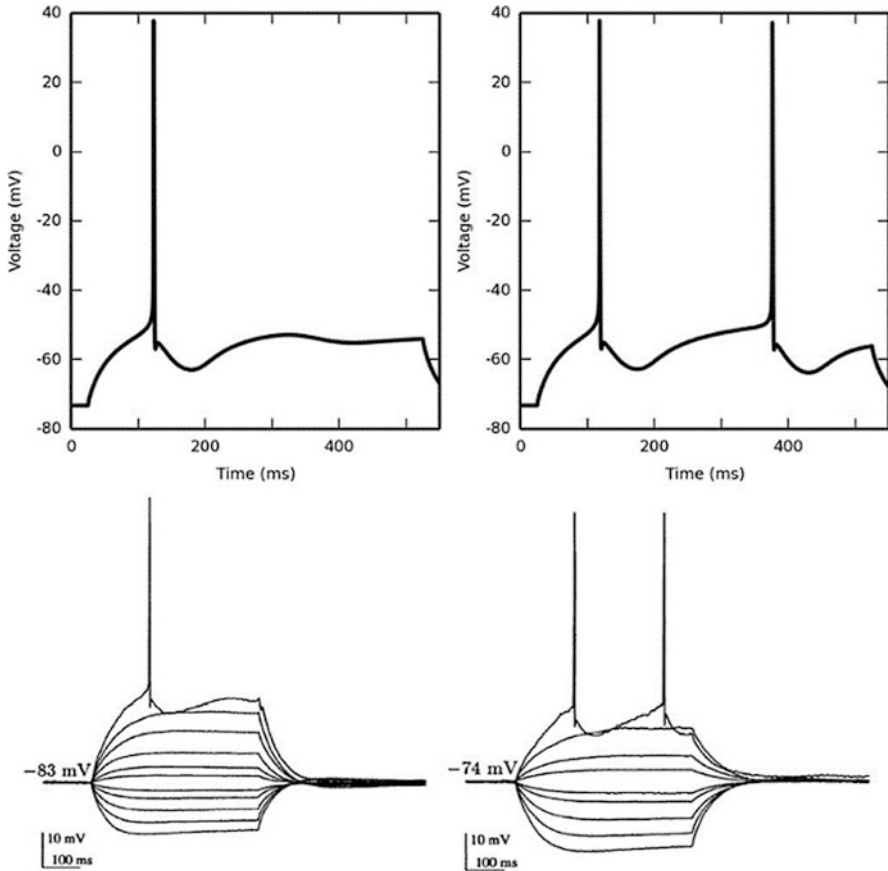


Fig. 4 Granule cell electrophysiology. Simulation results are on the top row. Experimental data are on the bottom row. (Top left) When current is injected at the soma, the granule cell responds by firing an action potential with a latency of approximately 100 ms. (Top right) When the current amplitude is just over the threshold required to elicit a second action potential, its latency is approximately 350 ms. This matches experimental data (bottom, reproduced from Spruston and Johnston 1992). Reproduced from Hendrickson et al. 2016 with permission.

of the axon, the postsynaptic region to which the axon is sent and, once the axon arrives at the postsynaptic region, the spatial distribution of the axon terminals. The next challenge after finding such data was the quantification of the work which was a nontrivial task due to the qualitative manner in which a majority of the works were presented. The key works that were used to constrain the projection from entorhinal cortex to dentate gyrus are detailed below.

Entorhinal-Dentate Topography

A major division of the entorhinal cortex is its separation into the medial and lateral regions. The projection of the axons from the entorhinal cortex to the hippocampus is termed the perforant path. An important topographical distinction between the medial and lateral entorhinal cortex is that upon reaching the dentate gyrus, the lateral perforant path terminates within the outer third of molecular layer and the medial perforant path terminates within the middle third (Hjorth-Simonsen and Jeune 1972; Witter 2007). This anatomical feature is preserved in the present model by limiting the respective connections to the appropriate regions of the granule cell morphologies.

A significant study by Dolorfo and Amaral (1998) was used to guide our models of the regional mappings from entorhinal cortex to the dentate gyrus. By injecting retrograde dye tracers in the dentate gyri of rats, the entorhinal origins of the cells projecting to those injection sites in the dentate were revealed. Injections were performed along the entire septo-temporal, or longitudinal, extent of the dentate, creating a thorough topographic map of the organization of entorhinal-dentate projections. Each injection was performed in a separate rat, and the result of the injection was presented as a grayscale heat map overlaid on a two-dimensional, flattened representation of the entorhinal cortex of the rat. The grayscale heat map represented the density of entorhinal neurons that projected to the injection site (Fig. 5).

Quantifying the data to use in the model proved a challenge due to the qualitative presentation of the results and the dissimilarity of brain shapes for each rat. To

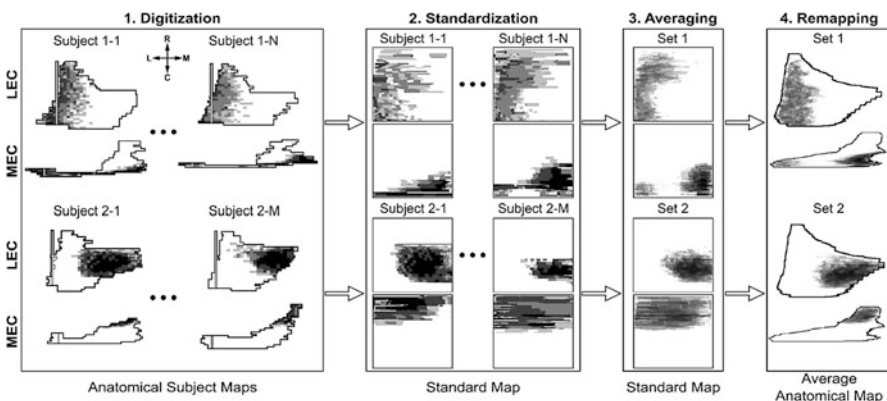


Fig. 5 Summary of the image-processing pipeline used to quantify the connectivity of entorhinal cortical projections to the dentate gyrus. Not all data are shown. (1) The data in the anatomical subject maps are digitized and grouped according to injection location. (2) The maps are projected onto a standard coordinate space. (3) The sets are averaged. (4) The averaged group data are projected onto an average anatomical map. The compass represents the rostro-caudal and mediolateral axes. Reproduced from Hendrickson et al. 2016 with permission.

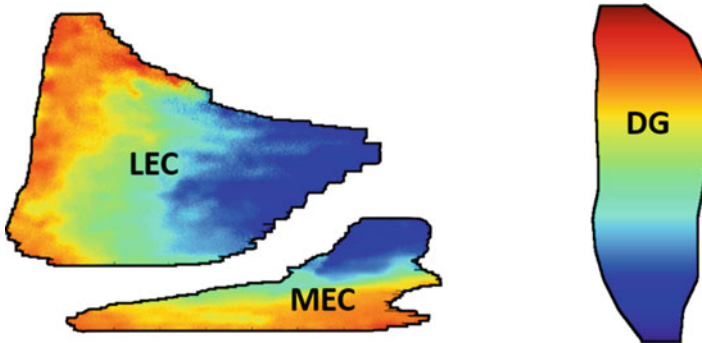


Fig. 6 Connectivity mapping from the lateral and medial entorhinal cortices (LEC and MEC) to the dentate gyrus (DG). Like colors between the entorhinal cortex and dentate gyrus correspond to the origin and destination of a projection, e.g., red entorhinal regions project to red dentate regions, blue entorhinal regions project to blue dentate regions, etc.

address this, a processing workflow was developed (Fig. 5). In the first step, the results of each injection were digitized, and the unique shape of the entorhinal cortex was extracted. Next, the individual entorhinal maps were transformed into a standard map, and the standardized maps were grouped based on the region of projection. The grouped, standardized maps were averaged, and the resulting averaged maps were transformed back to a representative entorhinal map that was created by calculating the average of all the entorhinal maps. The final grayscale heat maps were used to determine, given the origin of the neuron in the entorhinal cortex, the probabilistic location within the dentate gyrus to which the axon was connected. The final mapping depicts a mediolateral gradient in the lateral entorhinal cortex that projects along the longitudinal axis of the dentate gyrus. In the medial entorhinal cortex, there is a dorsoventral gradient that projects along the longitudinal axis of the dentate gyrus. A summary of the mapping is shown in Fig. 6.

The above study informed the regional mapping of the entorhinal-dentate projection, but it did not describe the morphology of the entorhinal axonal arbors. At the cellular level, Tamamaki and Nojyo (1993) produced some of the few reported single entorhinal neuron perforant path axon terminal reconstructions. Based on their work, the septo-temporal extent of the axon terminals was constrained to be in the range of 1–1.5 mm. Given that the axon terminals cover the entire transverse extent of the dentate gyrus, the entorhinal axons in the model were represented using Gaussian distributions with a standard deviation 0.167 mm which corresponds to approximately 1 mm being covered within three standard deviations from the center of the axon terminal field. These distributions determined the connectivity between the entorhinal neurons and the granule cells, providing the basis for feedforward excitation in this system.

Topography Within the Dentate Gyrus

Upon identifying a neuron and filling it with dye, septo-temporal cross sections of the hippocampus can be made, and the total length of axon that exists in the cross sections can be quantified. Such experiments have yielded histograms of the total axon length of a neuron as a function of distance away from the cell body. The histograms were fitted to Gaussian functions to extract the standard deviations that parameterize the spatial distributions of axon terminal fields of dentate granule cells and basket cells. The septo-temporal and transverse standard deviations for granule cells were estimated to be 0.152 mm and 0.333 mm, respectively (Patton and McNaughton 1995; Buckmaster and Dudek 1999). The corresponding standard deviations for basket cells were estimated to be 0.215 and 0.150 mm (Han et al. 1993; Sík et al. 1997). The resulting two-dimensional Gaussian distributions described the probability of connectivity between granule cells and basket cells.

The associational system of the dentate gyrus is provided by the mossy cells, and their axons extend predominantly into the inner third of the molecular layer (Buckmaster et al. 1996; Ribak and Shapiro 2007). Mossy cell axon terminals contact both granule cell and basket cell dendrites within the inner third (Scharfman et al. 1990; Scharfman 1995). The longitudinal extent of the axon terminal field is dependent on the location of their soma with fields that span 7.5 and 1.5 mm for mossy cells located septally and temporally, respectively (Zimmer 1971; Hendrickson et al. 2015).

Conduction Velocity of Action Potentials

To account for the time delay between the generation of an action potential and its arrival at the presynaptic terminal where it triggers neurotransmitter release, conduction velocity values, taken from the literature, and the Euclidean distance between the neurons were used. For the entorhinal conduction delays, a bifurcation point was assigned at the crest of the dentate gyrus at a longitudinal location according to topographic rules described earlier. The distance between the perforation point and the postsynaptic neuron was used to calculate the delay. The conduction velocity was estimated to be 0.3 m/s (Andersen et al. 1978).

Synaptic Density

The inputs to a postsynaptic neuron for each possible presynaptic cell type were determined by calculating the pairwise distance between the postsynaptic neuron and all of the presynaptic neurons and computing the connection probability using an appropriate probability distribution. Inputs were randomly selected until a threshold number of inputs, determined by the convergence value for the presynaptic cell type, were satisfied. The convergence value denotes the number of afferent

connections that a postsynaptic neuron receives from a given presynaptic neuron type and was estimated by considering the number of synapses that was available for a presynaptic neuron type. The determination of the convergence is detailed below.

Granule Cell Synapse Counts

Hama et al. (1989) quantified the spine density of granule cells by performing analyses on electron microscopy images of the granule cell dendrites. Though Hama et al. did not separately quantify the synaptic density based on the location of the granule cells with respect to the suprapyramidal and infrapyramidal blades of the dentate gyrus, Desmond and Levy (1985) reported significant differences between the blades. However, the methodology of Hama et al. was preferred as they used higher resolution electron microscopy imaging to perform the counting rather than light microscopy. Using the ratio of the spine densities between the blades as reported by Desmond and Levy, the spine densities for the infrapyramidal blade based on the work of Hama et al. were estimated. Furthermore, Crain et al. (1973) were able to identify asymmetric synapses in only a certain proportion of spines in the distal and middle dendrites, signifying excitatory synapses presumably from perforant path input. Claiborne et al. (1990) characterized the dendritic lengths of axons that lie in the various strata. With a total mean length of 3,478 μm for suprapyramidal granule cells and 2,793 μm for infrapyramidal granule cells and a mean of 30% of the dendrites in the middle third of the molecular layer and 40% in the distal third, the mean numbers of synapses available for the lateral and medial perforant path were computed as 2,417 and 2,117 for suprapyramidal granule cells and 1,480 and 1,253 for infrapyramidal cells, respectively (Table 4).

Halasy and Somogyi (1993) reported that 7–8% of synapses on granule cell dendrites in the molecular layer are GABA-immunopositive and these dendritic synapses represent 75% of the inhibitory synapses on granule cells with the remaining 25% located in the granule cell layer. Given total spine counts of 8,695 and 5,533 for suprapyramidal and infrapyramidal granule cells, respectively, the number of inhibitory inputs in the molecular layer would be 652 and 415. This would then leave 217 and 138 synapses in the granule cell layer. Basket cells send their axon collaterals predominantly to the granule cell layer, but they are not the only interneurons to do so. Chandelier cells, not included in this study, are hilar cells that also provide inhibitory input to the granule cell layer (Soriano and Frotscher 1989; Buhl et al. 1994). Given the average number of boutons between basket cells and chandelier cells, 11,400 and 3,800, approximately 75% of the synapses in the granule cell layer should be dedicated for basket cell input (Sik et al. 1997). The convergence of basket cells onto granule cells should then be 174 and 110 for the suprapyramidal and infrapyramidal granule cells. However, parvalbumin-positive basket cells only make up 62% of the basket cell population, so the convergence is appropriately shifted to 108 and 68, respectively (Buckmaster and Dudek 1997).

Table 4 Spine density and spine counts in granule cells

Property	Reference	Suprapiroamidal			Infrapiroamidal		
		Inner	Middle	Outer	Inner	Middle	Outer
Proportion of asymmetric synapses	Crain et al. (1973)	0.89	0.89	0.86	–	–	–
Spine density (spines/ μm)	Desmond and Levy (1985)	1.57	1.66	1.52	1.34	1.22	1.16
Number of spines	Hama et al. (1989)	3.36	2.28	2.02	2.87 ^a	1.68 ^a	1.54 ^a
	–	3,506	2,379	2,810	2,405	1,408	1,720
Number of asymmetric synapses	–	3,120	2,117	2,417	2,140	1,253	1,480

^aEstimated by calculating the supra- to infrapiroamidal ratio from the Desmond and Levy (1985) data.

Mossy cells have been reported to create 30,000–40,000 synapses within the inner third of the molecular layer (Buckmaster et al. 1996). Assuming that mossy cells maximally form one synapse per granule cell and there are 30,000 mossy cells and 1,200,000 granule cells, then a granule cell would receive an average of 875 mossy cell inputs. This number is less than the estimated number of spines in the inner molecular layer for granule cells (Table 4), but the mossy cell connections that were being investigated originated from ipsilateral connections and do not consider commissural input from the contralateral hippocampus.

Basket Cell Synapse Counts

The total dendritic length of dentate basket cells has been reported to be 4,530 μm . Of this length, the basal dendrites receive input from the granule cells. The proportion of dendrite that lies in the molecular layer (apical dendrites) versus the hilus (basal dendrites) was estimated from measurements of surface area with an apical surface area of 7,600 μm^2 and a basal surface area of 2,200 μm^2 (Vida 2010). The synaptic density for the dentate basket cell was taken from an estimate made by Patton and McNaughton (1995) which was 1 synapse/ μm . Another study reported that approximately 10% of synapses in CA1 basket cells are GABAergic (Gulyás et al. 1999). Using these data, the mean number of granule cell inputs for a basket cell was estimated to be 915. Assuming that the distribution of basket cell dendrites in the molecular layer was similar to that of granule cells, the number of lateral and medial entorhinal inputs for a basket cell was calculated to be 1,045 and 783, respectively. Similarly, the number of synapses in the inner third of the molecular layer was estimated to be 783. Considering that only a third of the inner molecular synapses of the granule cells were used for ipsilateral mossy cell connections, the same ratio was used for basket cells to estimate 260 mossy cell connections. Pyramidal basket cells also receive mossy cell input through its basal dendrites. Of the reported 2,700 synaptic contacts that mossy cells were found to make in the hilus, 60% was estimated to occur with inhibitory interneurons (Buckmaster et al. 1996; Wenzel et al. 1997). We assumed that all hilar interneurons have an equal probability of receiving a mossy cell input and that a hilar interneuron receives an average of two synaptic contacts from a single mossy cell (Buckmaster et al. 1996). Given a total hilar inhibitory interneuron population of 20,000 (Buckmaster and Jongen-Rêlo 1999), the estimated number of hilar mossy cell inputs to basket cells was 1,200. This would lead to a total number of mossy cell inputs to be 1,460.

Mossy Cell Synapse Counts

The present model only considers the granule cell input to mossy cells. Mossy cell excitation of other mossy cells and inhibitory inputs to mossy cells have yet to be included but are planned for future works. Acsády et al. (1998) reported that granule cells form synapses with 7–12 hilar mossy cells. Given a granule cell population of

Table 5 Parameters for AMPA synapses

	Granule cell	Basket cell	Mossy cell
Medial perforant path ^a			
g_{\max} (μS)	1.17e-5	4.21e-6	–
τ_1 (ms)	1.05	1.05	–
τ_2 (ms)	5.75	5.75	–
Convergence	2,117/1,253	783	–
Lateral perforant path ^a			
g_{\max} (μS)	1.50e-5	4.21e-6	–
τ_1 (ms)	1.05	1.05q	–
τ_2 (ms)	5.75	5.75	–
Convergence	2,417/1,480	1,045	–
Granule cell ^b			
g_{\max} (μS)	–	1.13e-4	2.00e-5
τ_1 (ms)	–	0.1	0.3
τ_2 (ms)	–	0.49	0.6
Convergence	–	915	380
Mossy cell ^c			
g_{\max} (μS)	1.17e-6	2.27e-5	–
τ_1 (ms)	1.05	1.05	–
τ_2 (ms)	5.75	0.49	–
Convergence	875	1,460	–

Presynaptic neurons are in the first column. Postsynaptic neurons are in the first row. The reversal potentials for AMPA synapses were 0 mV. The parameters for the postsynaptic potentials were optimized based on experimental data from the following papers: ^aFoster et al. (1991); ^bGeiger et al. (1997); and ^cScharfman (1995). Convergence values for granule cells are divided into supra- and infrapyramidal blades (supra/infra).

1,200,000 and a mossy cell population of 30,000, the estimated number of granule cell inputs that a mossy cell receives was 380. A summary of the convergence values is listed in Table 5.

Synaptic Model

In the currently described large-scale network, synapses were the exclusive mechanism through which neuron-to-neuron communication was mediated. The synapse was phenomenologically and deterministically represented so, upon being triggered by an action potential, the synaptic conductance would follow a time course dictated by a double exponential function according to the Exp2Syn mechanism in NEURON.

Table 6 Parameters for GABA_A synapses

	Granule cell	Basket cell	Mossy cell
Basket cell			
g_{\max} (μS)	1.24e-3	–	–
τ_1 (ms)	0.1	–	–
τ_2 (ms)	12.35	–	–
Convergence	108/68	–	–

Presynaptic neurons are in the first column. Postsynaptic neurons are in the first row. The reversal potentials for GABA synapses were -75 mV. The parameters for the postsynaptic potentials were optimized based on experimental data (Buhl et al. 1995).

$$g(t) \propto e^{-t/\tau_2} - e^{-t/\tau_1}$$

Though NMDA is crucial to synaptic plasticity, synaptic function for this implementation of the model was limited to AMPA, which allowed a base response of the neural network to be expressed and focused on the analysis on the two properties in question: topography and inhibition. Inhibitory GABAergic synapses for the present model were restricted to the GABA_A subtype and also were modeled using the Exp2Syn mechanism. The parameters of synapses between the various cell type pairs are summarized in Tables 5 and 6.

Simulation Results

Characterization of Baseline Dentate Response to Random Entorhinal Cortical Input

For our initial simulation study to characterize dentate granule cell responses to entorhinal input, the dentate network was driven using independent, identically distributed Poisson point processes which generated interstimulus intervals (ISIs) at a mean frequency of 3 Hz. The 3 Hz was chosen to represent a baseline of spontaneous activity for the entorhinal cortex. A Poisson process was used to generate ISIs that would perturb the synapses at a broad range of frequencies approximating a white noise input with which to investigate the entorhinal-dentate system. The resulting entorhinal activity was uncorrelated spatially and temporally. Once the inputs were generated, the same ISIs were used to perturb the network for all of the simulations that are described in this work.

The culmination of all of these steps resulted in the formation of a neural network approximating the entorhinal-dentate system of the hippocampus. Random, uncorrelated activity from the entorhinal cortex was projected to the dentate gyrus and spatially distributed according to experimentally established rules that

determine topographical connectivity. The activity was converted into postsynaptic potentials (PSPs) in the corresponding granule cells and basket cells based on the synaptic equations that determined the response. The PSPs were propagated through the dendritic morphologies, interacting with PSPs arising from other input timings and activating voltage-gated ion channels, resulting in a nonlinear transformation of the PSPs as they traveled toward, and were integrated at, the soma. Upon reaching a threshold, which was determined by the ion channel composition and density, the soma would generate an action potential which would activate neural circuits based on the local topography of the granule and basket cell axons and provoke a similar sequence of events from which large-scale population dynamics could be expressed in the form of spatiotemporal patterns of spiking. Initial simulations were performed at the full number of neurons in the entorhinal cortex and dentate gyrus (Table 1). To explore the various phenomena that were observed at the full-scale network, subsequent simulations were performed at a reduced scale with a tenth of the number of neurons to decrease the simulation times. Simulations performed at the reduced scale continued to exhibit the relevant phenomena seen at the full scale.

Simulations were performed on a computing cluster (hpc.usc.edu) using 125 dual quad-core 2.33 Ghz Intel-based nodes with 16 GB of RAM per node for a total of 1000 processor cores and 2 TB of RAM. The nodes were connected by a 10G Myrinet networking backbone. At full scale with 112,000 entorhinal cortex cells, 1,200,000 granule cells, and 4,000 basket cells with a simulation time of 4,000 ms, simulations required approximately 87 h to complete. Reduced scale simulations required approximately 9 h.

Spatiotemporal Clusters as an Emergent Property

The spiking activity of the network is depicted using raster plots with time on the x-axis. The entorhinal activity is sorted by cell ID which demonstrates the uncorrelated properties of its spatiotemporal firing pattern. For neurons in the dentate, the longitudinal location of a spike within the dentate is plotted on the y-axis. The basket cell activity is plotted similarly. The initial expectation was that spatiotemporally uncorrelated input from the entorhinal cortex would result in spatiotemporally uncorrelated output of granule cells. Contrary to that hypothesis, the dentate system responded with localized regions of spatially and temporally dense activity that were interspersed with periods of reduced activity. The dense activity spanned a spatial extent of 1–3 mm and persisted for approximately 50–75 ms with periods of reduced activity lasting 50–100 ms. Regions of dense activity were called “clusters” (Fig. 7).

The clustered activity was not a transient response but was the steady-state response after approximately 1 s of simulation had passed. The transient response was characterized by synchronized, oscillatory behavior (not shown). During this phase, the entire extent of the dentate gyrus alternated between periods of activity and inactivity before evolving into clustered activity which persisted indefinitely for

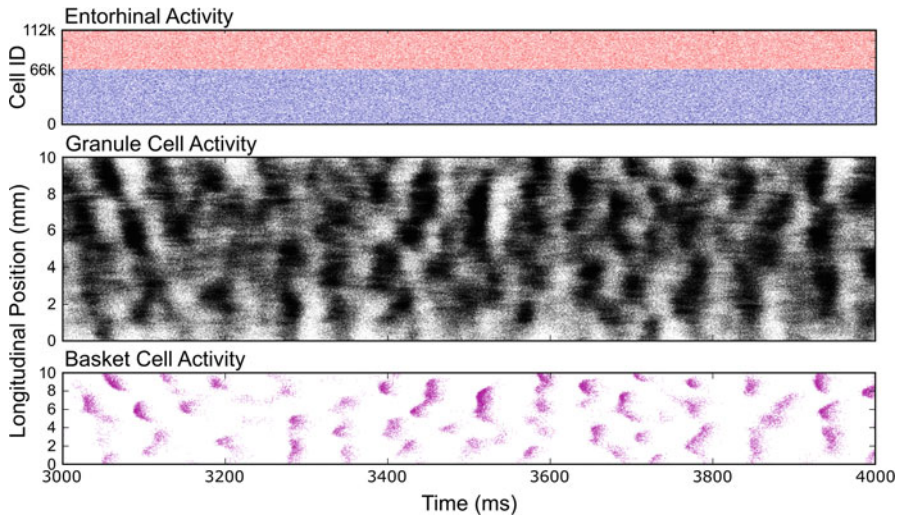


Fig. 7 Simulation result for topographically constrained entorhinal-dentate network with feedback inhibition at full scale with 1,200,000 granule cells. (Top) Entorhinal activity was generated by homogeneous Poisson process and was spatially and temporally uncorrelated. Medial entorhinal activity is in red and lateral entorhinal activity is in blue. (Middle) Granule cell activity displays spatiotemporal clustering with local regions of dense activity. (Bottom) Basket cell activity was also clustered, being driven, and activated in a feedback manner by granule cell activity

the rest of the simulation. Clusters persisted even after the network was scaled to one-tenth of the full scale (Fig. 9). The mean firing rate of the granule cells was 1.28 Hz.

A density-based clustering algorithm, DENCLUE 2.0 (Hinneburg and Gabriel 2007), was used to detect clusters for more in-depth characterization (Fig. 8). The mean number of spikes that contributed to each cluster in the reduced network was 156. Clusters had a mean temporal width of 18 ms and spatial extent of 0.90 mm. The mean density of the clusters was 12 spikes/ms•mm², and the intercentroid time between the clusters was 11 ms. Clusters were not formed due to bursts of spikes by individual granule cells. Rather, clusters were a result of increased population activity.

The clusters are an expression of a spatiotemporal correlation in the system. To test the robustness of this correlation, spatiotemporal correlation maps were computed in which the cross-correlations between cell pairs from the network were computed and the longitudinal distance between the cells was used to sort the correlations (Fig. 9). The spike times were sorted using a time bin of 5 ms, and the resolution of the cell distance was set to 0.05 mm. A uniform random sampling of 10,000 cells was performed, and the correlations were calculated with all unique cell pair combinations from this sampling. The resulting maps capture the average features of the clusters that are apparent visually and verify the existence of a

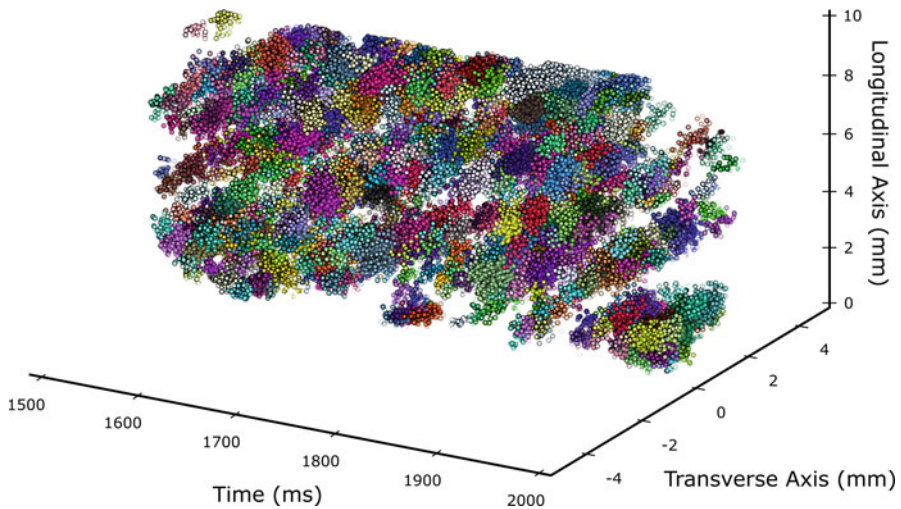


Fig. 8 DENCLUE analysis of granule cell-spiking activity which identifies clusters based on the local density. Each identified cluster is plotted with a separate color. The cluster analysis shows that clusters are organized by the transverse axis in addition to the longitudinal and temporal axes

spatiotemporal correlation in the dentate population which was not present in the entorhinal population.

Removal of Extrinsic and Intrinsic Sources of Inhibition

To identify the properties that were responsible for the spatiotemporal correlation, physiological components were successively removed until the clusters were substantially modified or no longer detected. The initial hypothesis was that the clusters were formed due to sources of inhibition. First, basket cells were considered as an extrinsic source of inhibition due to the inhibitory feedback they provide to granule cells. The dynamics of inhibition and spatial distribution of fibers should generally correspond to the inter-cluster timing and cluster size. The removal of basket cells from the network increased the level of background activity or “noise” in the system but changed the shape of clusters only subtly (Fig. 9). Next, an intrinsic source of inhibition was investigated, the afterhyperpolarization (AHP) of granule cells. The reduced spiking during the AHP could contribute to the reduced inter-cluster activity. The amplitude of the fast AHP of the granule cells was reduced by half, and the half-height width was reduced by one-third by removing the calcium-dependent potassium conductances (the small conductance calcium-activated potassium channel, SK, and the large conductance calcium-activated potassium channel, BK). In the absence of basket cell inhibition and the AHP, a greater amount of noise was present making clusters more difficult to detect visually, but the correlation maps continued to demonstrate the presence of a substantial

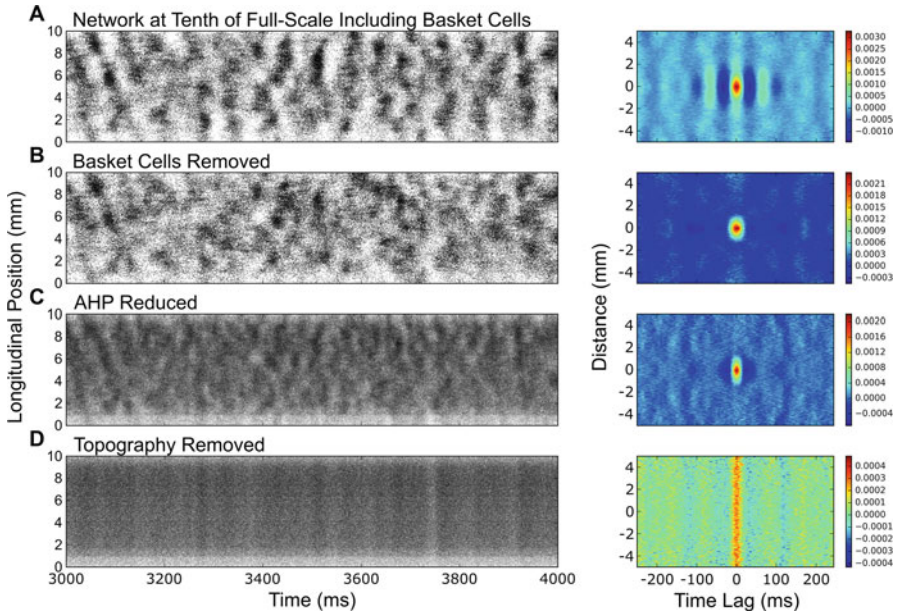


Fig. 9 Raster plots of activity from an entorhinal-dentate network at 1/10th of the full scale while cumulatively removing extrinsic and intrinsic sources of inhibition as well as topographical connectivity constraints. The corresponding correlation maps are to the right of each raster plot. (a) Clustered activity persists in a network that is scaled down. The correlation map exhibits spatial and temporal correlation that matches the size and extent of the dentate clusters. (b) Basket cells are removed as a source of extrinsic inhibition, but clustered activity remains. (c) Extrinsic and intrinsic sources of inhibition are eliminated by reducing the AHP amplitude and removing basket cells. Background activity increases, but clusters are still present. (d) In the absence of basket cells and AHP, entorhinal cortical cells and granule cells are randomly connected to eliminate topography. It is only after topographical connectivity constraints are removed that the clusters disappear

spatiotemporal correlation (Fig. 9). Both of these simulations indicated that clusters were not a result of neurobiological mechanisms that contribute to the inhibition of granule cell activity.

Topographic Connectivity as a Source of Spatial Correlation

The next simulation sought to eliminate topography. With topography, entorhinal cortical cells exhibited an axon terminal field that spanned a longitudinal extent of 1 mm, constraining their postsynaptic targets to granule cells within this extent. Topography was removed by using a random connectivity; entorhinal cortical cells were allowed to synapse with any dentate granule cell with equal probability. Each

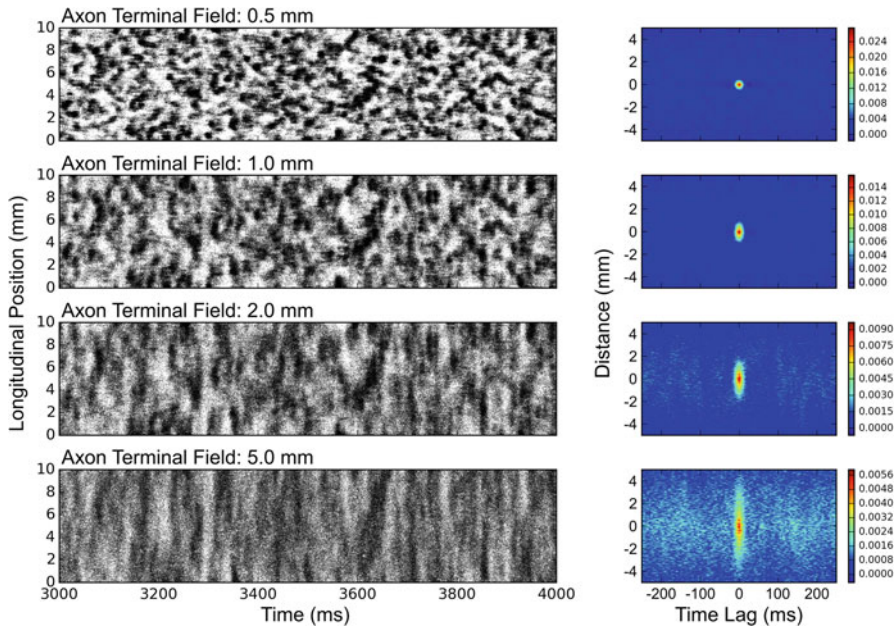


Fig. 10 Effect of increasing the axon terminal field extent in the septo-temporal direction. Raster plots of the granule cell activity are in the left column. Correlation maps are plotted on the right. As the terminal field extent is increased, the cluster size is increased, and this is further reflected by the expanding spatial extent of the correlation

neuron received the same number of connections as before, but the potential origin of the inputs was entirely random. The result of removing the topography of the entorhinal projection, in the absence of basket cells and a reduced AHP, was the elimination of clustered activity (Fig. 9). This result demonstrated that the spatial correlation and clusters are primarily dependent on the topography of the entorhinal-dentate system.

Given that both the spatial extent of the clusters and the span of the axon terminal field were approximately 1 mm, it was presumed that the axon terminal field could be acting as a spatial filter that controlled the spatial correlation in the population activity. To test this hypothesis, the axon terminal field of the entorhinal-dentate projection was varied from 0.5 to 5 mm (Fig. 10). Basket cells were not included in these simulations, and the granule cell models were restored to their original ion channel composition, i.e., amplitudes of AHPs were not reduced. The simulations verified that the extent of the axon terminal field determines the spatial extent of the clustered activity. However, the temporal extent of the clusters was not affected by the axon terminal field.

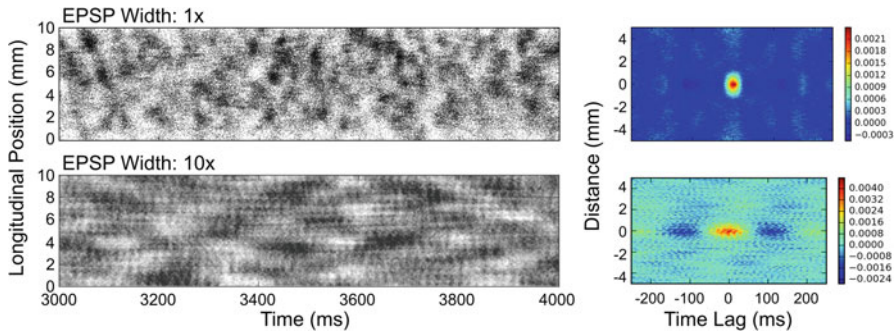


Fig. 11 Granule cell activity if the time course of the entorhinal-dentate EPSP is expanded. Fewer clusters were seen in the granule cell activity, but the temporal width of the clusters increased. This is also seen in the correlation map

Sources of Temporal Correlation

Though extrinsic and intrinsic sources of inhibition, i.e., basket cells and AHP, were not found to be the source of clusters, they were able to modulate the appearance of the clusters and the temporal aspect of the correlation maps (Fig. 9). In particular, they affected the regions of negative correlation that appeared on either sides of the positive correlation lobes. However, neither processes significantly changed the width of the lobes. We hypothesized that by changing the temporal properties of the EPSP, the temporal width of both the clusters and correlation could be manipulated. The second time constant τ_2 of the double exponential equation that describes the synaptic dynamics primarily influences the width of the resulting PSP. To extend the temporal width of the PSP, τ_2 was increased by a factor of 10. The first time constant τ_1 primarily affects the rise time of the PSP and was not manipulated for this simulation. In order to maintain similar levels of activity, the amplitude of the EPSP was altered such that its integral remained unchanged with respect to the original, experimentally based EPSP waveform. The population responded with wider but fewer clusters that appeared with a different spatiotemporal pattern than the control. The simulations verified that the temporal extent of the clusters and correlation were proportional to the temporal extent of the EPSP (Fig. 11).

Modulation of Clusters via Interneurons

The model of the dentate gyrus used in the present studies was comprehensive, particularly with respect to the morphologies of granule cells, topographic organization of perforant path fibers, biophysical properties of granule cell bodies and dendrites, relative numbers of granule cells and basket cell inhibitory interneurons, total numbers of neurons included in the model, and other prominent features known to be characteristic of the hippocampal entorhinal-dentate system in the

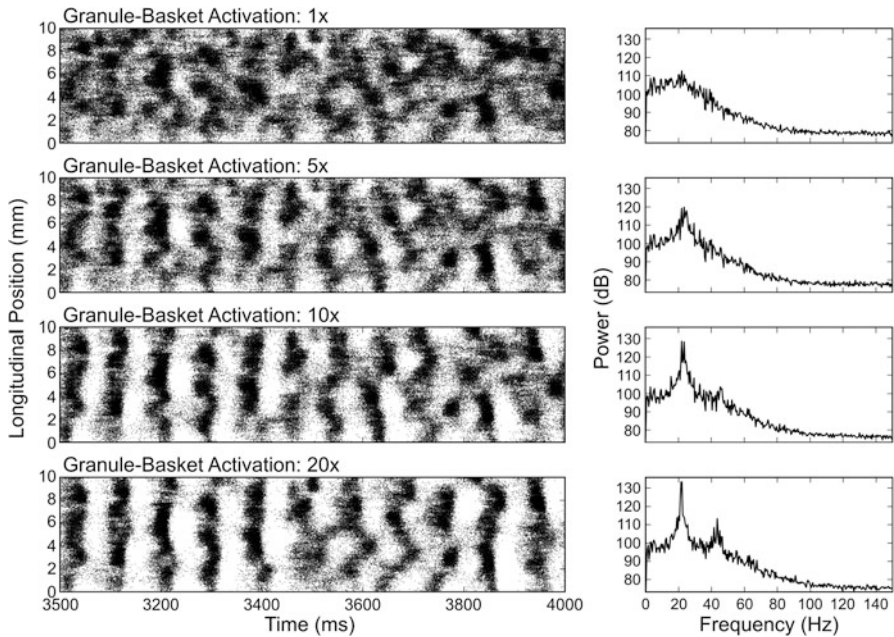


Fig. 12 Results of increasing the strength of feedback inhibition. As feedback inhibition increased, synchrony increased and oscillatory behavior became apparent. The Fourier transforms depict a strengthening of oscillation at 22 Hz. Reproduced from Hendrickson et al. 2016 with permission

rat. In addition, and relevant to the current volume, in the present model, we have investigated the role of basket cells forming feedforward and feedback inhibitory pathways and mossy cells contributing feedback from the hilus to granule cells and inhibitory interneurons (Hendrickson et al. 2015, 2016). Positive feedback was mediated by mossy cells which monosynaptically provided excitatory input to granule cells but also disynaptically provoked an inhibitory effect by activating basket cells.

The role of feedback inhibition was investigated by increasing the strength of basket cell activation by granule cells and observing the granule cell activity. As the coupling strength was increased, the clustered activity began to align temporally (Fig. 12). At higher coupling strengths, the aligned clusters became joined into a single vertical band, and the granule cell activity appeared as an oscillation between periods of activity and inactivity. The oscillation frequency of the synchronous activity was evaluated using Fourier analysis which exhibited a primary peak at 22 Hz and, at the higher coupling strengths, a resonant peak at 45 Hz.

Feedforward inhibition was investigated by increasing the strength of basket cell activation by entorhinal cortical cells and observing granule cell activity. Alone, feedforward inhibition acted to dampen activity and eventually ceased any granule cell activity from occurring at higher coupling strengths (figure not shown). The

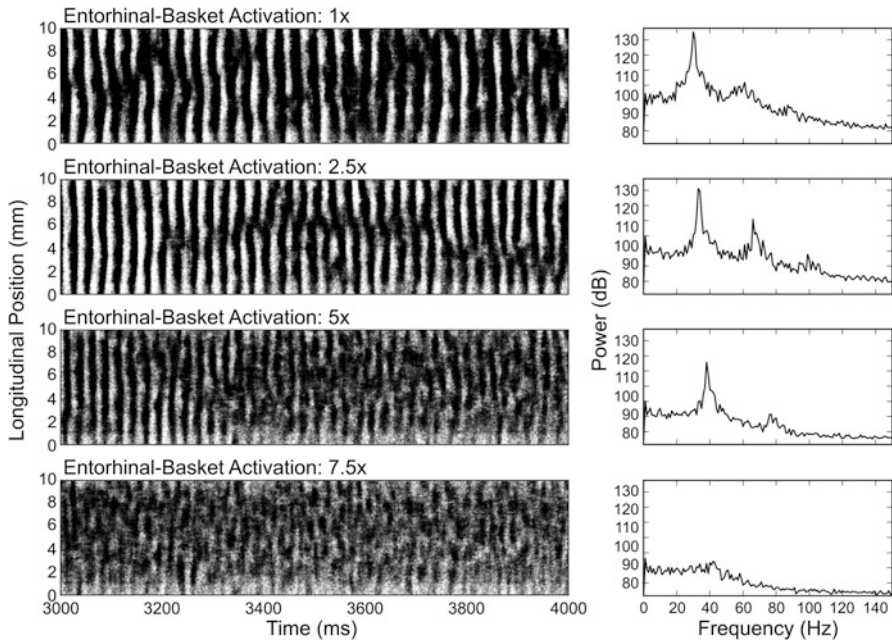


Fig. 13 Results of increasing the strength of feedforward inhibition while the network was in an oscillatory state due to feedback inhibition. As feedforward inhibition was increased, the oscillation frequency increased, but beyond a certain level, oscillatory activity was dampened, and the granule cells begin to exhibit clustered activity

interactions between feedforward and feedback inhibition then were explored (Fig. 13). The strength of feedback inhibition was set such that granule cells exhibited a 22 Hz oscillation. In this state, the entorhinal-basket cell coupling strength was steadily increased. At lower coupling strengths, the 22 Hz oscillation was shifted toward higher frequencies, but beyond a certain level, the peak oscillation was weakened and eventually eliminated, reverting to clustered activity.

Mossy cells were found to affect the shape of the clusters and the prevalence of excitatory activity in the network. Clusters were denser and started and terminated more sharply (Fig. 14). Larger clusters that spanned 4–6 mm of the longitudinal extent of the dentate also began to appear. The introduction of mossy cells further introduced a global oscillation dynamic in that the system would alternate between a period of strong and densely packed clusters and a period of weaker and more dispersed clusters. A Fourier analysis showed that the oscillation occurred in the low theta region in the range of 2–5 Hz. By manipulating the synaptic strength between the mossy-granule cell projection and the mossy-basket cell projection, the dentate network could be easily induced to enter an aberrant bursting state reminiscent of epileptic activity (Fig. 14). Changing the strengths by a factor of 2 was sufficient to elicit a bursting response during the strong cluster period. The results support both the “irritable mossy cell” hypothesis, which proposes a strengthened coupling

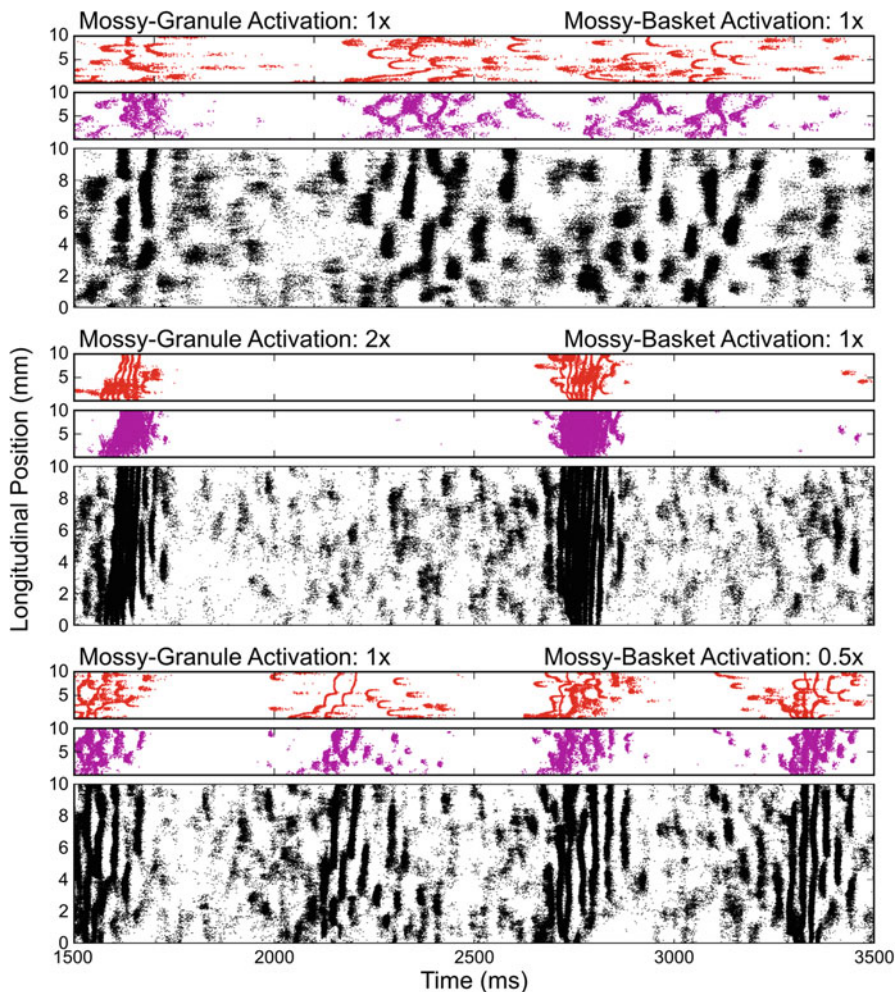


Fig. 14 Dentate activity in a network containing granule cells (black), basket cells (magenta), and mossy cells (red). A global oscillation is seen where the network responds with periods of strong and dense clusters and periods of weak and sparse clusters. When the strength of the mossy-granule cell synapses is increased, the strong cluster period exhibits epileptic activity. Similarly, when the strength of the mossy-basket cell synapses is decreased, the strong cluster period exhibits epileptic activity

between mossy cells and granule cells, and the “dormant basket cell” hypothesis, which proposes a weakened coupling between mossy cells and basket cells, that both explain a network level mechanism behind epilepsy (Santhakumar et al. 2000; Sloviter et al. 2003; Dyhrfjeld-Johnsen et al. 2007). Morgan and Soltesz (2010) developed a large-scale model of the dentate gyrus to investigate a biologically plausible mechanism by which the hyperexcitability seen in epilepsy could be

generated. Injury was simulated by adding granule cell-to-granule cell connections, a phenomenon called mossy fiber sprouting, and reducing the number of mossy cells in the network. Their study demonstrated that the formation of hub cells, highly connected granule cells with large numbers of incoming and outgoing connections, may explain hyperexcitability in epilepsy.

The relatively wide range of network parameters associated with the network tendency for high levels of excitability and epileptiform firing also demonstrates the difficulty in controlling a network as its complexity grows. Strictly from a modeling and simulation standpoint, this may be particularly troublesome given that computational studies of the hippocampus and other brain systems will increasingly seek to include greater and greater numbers of interconnects and neuron types to achieve biological completeness.

The additional hierarchical organization imposed by the mossy cells and basket cells resulted in a more unstable system which raises more questions on the role of hierarchies in a complex network and how stability is maintained in such systems. The investigations reviewed here lacked other key dentate interneurons such as chandelier, HICAP, HIPPO, IS, and MOPP cells which, to complete the dentate network, will be included in future studies. Their inclusion will undoubtedly introduce many more sources of instability as the number of hierarchical circuit interactions grows, but understanding the intricacies of such a network will offer important insights into the conditions generating abnormal dentate system activity, as well as suggesting mechanisms behind disease states.

Discussion and Future Work

Spatiotemporal Clusters as a Higher Level of Functional Organization

The large-scale model introduced here offers one of the few insights into *in vivo* population dynamics by incorporating an anatomically derived connectivity and large numbers of detailed, biologically realistic neuron models. The emergence of spatially and temporally finite clusters in the spiking activity, indicative of a spatiotemporal correlation in the network, is a unique discovery that has yet to be validated experimentally but remains an hypothesis highly suggestive of how population activity could be organized at a higher level in the hippocampal dentate system. Topography, terminal field size, and synaptic communication are integral properties that underlie all neural systems and were found to significantly influence the shape of the clusters. The fundamental nature of topography, terminal fields, and synaptic transmission suggests that clusters could be found in many neural systems and that clusters may act as a basic unit of neuronal activity at the population level.

Though the correlation maps were able to be computed through averaging, the magnitude of the correlations was relatively low for all simulation cases. Clusters

could be visualized or detected only because of the scale of the network in terms of the geometry and the number of neurons. A network that is restricted in scale to that of a typical 400 μm hippocampal *in vitro* slice would not exhibit clustered activity because the spatial extent of the system would be insufficient to observe the spatial boundaries of a cluster which are approximately 1 mm. Without having constructed a network of the magnitude reported here, the number of observable spikes would not be sufficient to calculate the correlations. As described above, the clusters themselves are sparse, with an average of 156 spikes per cluster. This is not to suggest that the clusters represent a minor aspect of granule cell activity but rather to emphasize that the phenomena would otherwise be overlooked had a large-scale network not been constructed.

Propagation and Transformation of Clusters

By extending the model beyond the dentate gyrus and incorporating the CA3/4 and CA2/1 subfields, the propagation and transformation of the granule cell clusters will be investigated in future studies (Yu et al. 2015). Because the topography of the projections between each of the subfields is unique, multiple connectivity schemes will be tested and compared. The mossy fibers, which are composed of the axonal projection from the dentate granule cells to the CA3/4 pyramidal cells, originate from a large presynaptic population and have a low divergence on the postsynaptic population, i.e., each granule cell contacts 11–15 CA3 pyramidal cells (Acsády et al. 1998). Conversely, the entorhinal projections to CA3 (projections do not extend to CA4) have high divergence values similar to the entorhinal-dentate projection. Within the CA3 region, there is an extensive, widely diverging associational system. Finally, the Schaffer collaterals that describe the CA3/4 projection to CA1 contain axon terminal fields that span large portions of the CA1 subfield (Ishizuka et al. 1990). An implementation of the entorhinal-dentate-CA3 topography has already been constructed, and so many of these studies are already underway (Yu et al. 2014).

Behaviorally Relevant Inputs to the Hippocampus

In the current studies, entorhinal cortical activity has been represented using homogeneous Poisson processes based on white noise system identification principles, but this activity is nonphysiological. Toward implementing a behaviorally relevant input for the hippocampal neural network, the activity of grid cells in the medial entorhinal cortex (Hafting et al. 2005) is being modeled using experimentally based rate maps and heterogeneous Poisson processes (Yu et al. 2016). Using this input paradigm, the lower levels of hippocampal dynamics can be linked to an even higher-level function toward the behavioral level: the encoding of

spatial information. Using the network generated by our framework, the biological determinants of spatial encoding and spatial processing can be explored. The network model can also be used to explore spatial processing in the context of other proposed functions of the hippocampal subfields such as pattern separation and pattern completion.

Acknowledgments This work was supported by ONR Grant N00014-13-1-0211, NIBIB Grant P41 EB001978, and NIH Grant U01 GM104604. Computation for the work was supported by the University of Southern California Center for High-Performance Computing and Communications (www.usc.edu/hpcc).

References

- Acsády L, Kamondi A, Sík A, Freund TF, Buzsáki G (1998) GABAergic cells are the major postsynaptic targets of mossy fibers in the rat hippocampus. *J Neurosci* 19:3386–3403
- Acsády L, Katona I, Martínez-Guijarro FJ, Buzsáki G, Freund TF (2000) Unusual target selectivity of perisomatic inhibitory cells in the hilar region of the rat hippocampus. *J Neurosci* 20:6907–6919
- Aggleton JP, Brown MW (1999) Episodic memory, amnesia, and the hippocampal-anterior thalamic axis. *Behav Brain Sci* 22:425–444
- Andersen P, Bliss TVP, Skrede KK (1971) Lamellar organization of hippocampal excitatory pathways. *Exp Brain Res* 13:222–238
- Andersen P, Silfvenius H, Sundberg SH, Sveen O, Wigström H (1978) Functional characteristics of unmyelinated fibres in the hippocampal cortex. *Brain Res* 144:11–18
- Aradi I, Holmes WR (1999) Role of multiple calcium and calcium-dependent conductances in regulation of hippocampal dentate granule cell excitability. *J Comput Neurosci* 6:215–235
- Aradi I, Soltesz I (2002) Modulation of network behaviour by changes in variance in interneuronal properties. *J Phys* 539:227–251
- Ascoli GA, Krichmar JL (2000) L-neuron: a modeling tool for the efficient generation and parsimonious description of dendritic morphology. *Neurocomputing* 32-33:1003–1011
- Ascoli GA, Donohue DE, Halavi M (2007) NeuroMorpho.Org: a central resource for neuronal morphologies. *J Neurosci* 27:9247–9251
- Berger TW, Bassett JL (1992) System properties of the hippocampus. In: Gormezano I, Wasserman EA (eds) *Learning and memory: the biological substrates*. Lawrence Erlbaum, Hillsdale, pp 275–320
- Berger TW, Weisz DJ (1987) Single unit analysis of hippocampal pyramidal and granule cells during classic conditioning of the rabbit nictitating membrane response. In: Gormezano I, Prokasy WF, Thompson RF (eds) *Classical conditioning III: behavioral, neurophysiological and neurochemical studies in the rabbit*. Lawrence Erlbaum, Hillsdale, pp 217–253
- Berger TW, Semple-Rowland S, Bassett JL (1981) Hippocampal polymorph neurons are the cells of origin for ipsilateral association and commissural afferents to the dentate gyrus. *Brain Res* 215:329–336
- Berger TW, Rinaldi P, Weisz DJ, Thompson RF (1983) Single unit analysis of different hippocampal cell types during classical conditioning of the rabbit nictitating membrane response. *J Neurophysiol* 50:1197–1219
- Berger TW, Berry SD, Thompson RF (1986) Role of the hippocampus in classical conditioning of aversive and appetitive behaviors. In: Isaacson RL, Pribram KH (eds) *The hippocampus*, vol 4. Plenum, New York, pp 203–239

- Berger TW, Hampson RE, Song D, Goonawardena A, Marmarelis VZ, Deadwyler SA (2011) A cortical neural prosthesis for restoring and enhancing memory. *J Neural Eng* 8:046017. <https://doi.org/10.1088/1741-2560/8/4/046017>
- Buckmaster PS, Dudek FE (1997) Neuron loss, granule cell axon reorganization, and functional changes in the dentate gyrus of epileptic kainate-treated rats. *J Comp Neurol* 385:385–404
- Buckmaster PS, Dudek FE (1999) In vivo intracellular analysis of granule cell axon reorganization in epileptic rats. *J Neurophysiol* 81:712–721
- Buckmaster PS, Jongen-Rêlo AL (1999) Highly specific neuron loss preserves lateral inhibitory circuits in the dentate gyrus of kainite-induced epileptic rats. *J Neurosci* 19:9519–9529
- Buckmaster PS, Strowbridge BW, Kunkel DD, Schmiede DL, Schwartzkroin PA (1992) Mossy cell axonal projections to the dentate gyrus molecular layer in the rat hippocampal slice. *Hippocampus* 2:349–362
- Buckmaster PS, Wenzel HJ, Kunkel DD, Schwartzkroin PA (1996) Axon arbors and synaptic connections of hippocampal mossy cells in the rat in vivo. *J Comp Neurol* 366:271–292
- Buhl EH, Halasy K, Somogyi P (1994) Diverse sources of hippocampal unitary inhibitory postsynaptic potentials and the number of synaptic release sites. *Nature* 368:823–828
- Buhl EH, Cobb SR, Halasy K, Somogyi P (1995) Properties of unitary IPSPs evoked by anatomically identified basket cells in the rat hippocampus. *Eur J Neurosci* 7:1989–2004
- Cajal SR (1968) *The structure of the Ammon's horn*. Charles C. Thomas, Springfield
- Carnevale NT, Hines ML (2006) *The NEURON book*. Cambridge University Press, Cambridge
- Claiborne BJ, Amaral DG, Cowan WM (1990) Quantitative, three-dimensional analysis of granule cell dendrites in the rat dentate gyrus. *J Comp Neurol* 302:206–219
- Cohen NJ, Eichenbaum H (1993) *Memory, amnesia and the hippocampal system*. MIT Press, Cambridge
- Crain B, Cotman C, Taylor D, Lynch G (1973) A quantitative electron microscopic study of synaptogenesis in the dentate gyrus of the rat. *Brain Res* 63:195–204
- De Schutter E, Bower JM (1994) An active membrane model of the cerebellar Purkinje cell I. Simulation of current clamps in slice. *J Neurophysiol* 71:375–400
- Desmond NL, Levy WB (1985) Granule cell dendritic spine density in the rat hippocampus varies with spine shape and location. *Neurosci Lett* 54:219–224
- Dolorfo CL, Amaral DG (1998) Entorhinal cortex of the rat: topographic organization of the cells of origin of the perforant path projection to the dentate gyrus. *J Comp Neurol* 398:25–48
- Douglas RM, McNaughton BL, Goddard GV (1983) Commissural inhibition and facilitation of granule cell discharge in fascia dentata. *J Comp Neurol* 219:285–294
- Dyhrfjeld-Johnsen J, Santhakumar V, Morgan RJ, Huerta R, Tsimring L, Soltesz I (2007) Topological determinants of epileptogenesis in large-scale structural and functional models of the dentate gyrus derived from experimental data. *J Neurophysiol* 97:1566–1587
- Eichenbaum H, Wiener SI, Shapiro ML, Cohen NJ (1989) The organization of spatial coding in the hippocampus: a study of neural ensemble activity. *J Neurosci* 9:2764–2775
- Foster TC, Barnes CA, Rao G, McNaughton BL (1991) Increase in perforant path quantal size in aged F-344 rats. *Neurobiol Aging* 12:441–448
- Freund TF, Buzsáki G (1996) Interneurons of the hippocampus. *Hippocampus* 6:347–470
- Gaarskjaer FB (1978) Organization of the mossy fiber system of the rat studied in extended hippocampi I: terminal area related to number of granule and pyramidal cells. *J Comp Neurol* 178:49–71
- Gamrani H, Onteniente B, Seguela P, Geffard M, Calas A (1986) Gamma-aminobutyric acid-immunoreactivity in the rat hippocampus: a light and electron microscopic study with anti-GABA antibodies. *Brain Res* 364:30–38
- Geiger JRP, Lübke J, Roth A, Frotscher M, Jonas P (1997) Submillisecond AMPA receptor-mediated signaling at a principal neuron-interneuron synapse. *Neuron* 18:1009–1023
- Gottlieb DI, Cowan WM (1973) Autoradiographic studies of the commissural and ipsilateral association connection of the hippocampus and dentate gyrus of the rat. I. The commissural connections. *J Comp Neurol* 149:393–421

- Gulyás AI, Megías M, Emri Z, Freund TF (1999) Total number and ratio of excitatory and inhibitory synapses converging onto single interneurons of different types in the CA1 area of the rat hippocampus. *J Neurosci* 19:10082–10097
- Hafting T, Fyhn M, Molden S, Moser M-B, Moser EI (2005) Microstructure of a spatial map in the entorhinal cortex. *Nature* 436:801–806. <https://doi.org/10.1038/nature03721>
- Halasy K, Somogyi P (1993) Distribution of GABAergic synapses and their targets in the dentate gyrus of rat: a quantitative immunoelectron microscopic analysis. *J Hirnforsch* 34:299–308
- Hama K, Arii T, Kosaka T (1989) Three-dimensional morphometrical study of dendritic spines of the granule cell in the rat dentate gyrus with HVEM stereo images. *J Electron Microscop Tech* 12:80–87
- Hampson RE, Simeral JD, Deadwyler SA (1999) Distribution of spatial and nonspatial information in dorsal hippocampus. *Nature* 402:610–614
- Han ZS, Buhl EH, Lörinczi Z, Somogyi P (1993) A high degree of spatial selectivity in the axonal and dendritic domains of physiologically identified local-circuit neurons in the dentate gyrus of the rat hippocampus. *Eur J Neurosci* 5:395–410
- Hasselmo ME (2005) What is the function of hippocampal theta rhythm?—linking behavioral data to phasic properties of field potential and unit recording data. *Hippocampus* 15:936–949. <https://doi.org/10.1002/hipo.20116>
- Hendrickson PJ, Yu GJ, Song D, Berger TW (2015) Interactions between inhibitory interneurons and excitatory associational circuitry in determining spatio-temporal dynamics of hippocampal dentate granule cells: a large-scale computational study. *Front Syst Neurosci* 9. <https://doi.org/10.3389/fnsys.2015.00155>
- Hendrickson PJ, Yu GJ, Song D, Berger TW (2016) A million-plus neuron model of the hippocampal dentate gyrus: critical role for topography in determining spatiotemporal network dynamics. *IEEE Trans Biomed Eng* 63:199–209
- Hines ML, Davison AP, Muller E (2009) NEURON and Python. *Front Neuroinform* 28. <https://doi.org/10.3389/neuro.11.001.2009>
- Hinneburg A, Gabriel H (2007) DENCLUE 2.0: fast clustering based on kernel density estimation. In *Proceedings of the 7th international conference on advances in intelligent data analysis*, Ljubljana, vol. 4723, pp 70–80
- Hjorth-Simonsen A, Jeune B (1972) Origin and termination of the hippocampal perforant path in the rat studied by silver impregnation. *J Comp Neurol* 144:215–232
- Ishizuka N, Weber J, Amaral DG (1990) Organization of intrahippocampal projections originating from CA3 pyramidal cells in the rat. *J Comp Neurol*. 295:580–623
- Jaffe DB, Ross WN, Lisman JE, Lasser-Ross N, Miyakawa H, Johnston D (1994) A model for dendritic Ca²⁺ accumulation in hippocampal pyramidal neurons based on fluorescence imaging measurements. *J Neurosci* 14:1065–1077
- Krueppel R, Remy S, Beck H (2011) Dendritic integration in hippocampal dentate granule cells. *Neuron* 71:512–528
- Krupic J, Burgess N, O'Keefe J (2012) Neural representations of location composed of spatially periodic bands. *Science* 337:853–857
- Levy WB (1989) A computational approach to hippocampal function. In: *Psychology of learning and motivation*. Elsevier, pp 243–305
- Lorente de Nó R (1934) Studies on the structure of the cerebral cortex II: continuation of the study of the ammonic system. *J Psychol Neurol* 46:113–177
- MacKenzie S, Frank AJ, Kinsky NR, Porter B, Rivière PD, Eichenbaum H (2014) Hippocampal representation of related and opposing memories develop within distinct, hierarchically organized neural schemas. *Neuron* 83:202–215
- McClelland JL, McNaughton BL, O'Reilly RC (1995) Why there are complementary learning systems in the hippocampus and neocortex: insights from the successes and failures of connectionist models of learning and memory. *Psychol Rev* 102:419–457. <https://doi.org/10.1037/0033-295x.102.3.419>

- McNaughton BL, Morris RGM (1987) Hippocampal synaptic enhancement and information storage within a distributed memory system. *Trends Neurosci* 10:408–415. [https://doi.org/10.1016/0166-2236\(87\)90011-7](https://doi.org/10.1016/0166-2236(87)90011-7)
- Marr D (1971) Simple memory: a theory for archicortex. *Philos Trans R Soc Lond* 262:23–81
- Morgan RJ, Soltesz I (2010) Microcircuit model of the dentate gyrus in epilepsy. In: Cutsuridis V, Graham BP, Cobb S, Vida I (eds) *Hippocampal microcircuits*. Springer, New York, pp 495–525
- Mulders WHAM, West MJ, Slomianka L (1997) Neuron numbers in the presubiculum, parasubiculum, and entorhinal area of the rat. *J Comp Neurol* 385:83–94
- Myers CE, Scharfman HE (2011) Pattern separation in the dentate gyrus: a role for the CA3 backprojection. *Hippocampus* 21:1190–1215
- Nadel L, Moscovitch M (1997) Memory consolidation, retrograde amnesia and the hippocampal complex. *Curr Opin Neurobiol* 7:217–227
- O’Keefe J, Nadel L (1978) *The Hippocampus as a cognitive map*. Oxford University Press, London
- Oliphant TE (2007) Python for scientific computing. *Comput Sci Eng* 9:10–20
- Patton PE, McNaughton BL (1995) Connection matrix of the hippocampal formation: I. The dentate gyrus. *Hippocampus* 5:245–286
- Ribak CE, Seress L (1983) Five types of basket cell in the hippocampal dentate gyrus: a combined Golgi and electron microscopic study. *J Neurocytol* 12:577–597
- Ribak CE, Shapiro LA (2007) Ultrastructure and synaptic connectivity of cell types in the adult rat dentate gyrus. *Prog Brain Res* 163:155–166
- Ribak CE, Nitsch R, Seress L (1990) Proportion of parvalbumin-positive basket cells in the GABAergic innervation of pyramidal and granule cells of the rat hippocampal formation. *J Comp Neurol* 300:449–461
- Rihn LL, Claiborne BJ (1990) Dendritic growth and regression in rat dentate granule cells during late postnatal development. *Dev Brain Res* 54:115–124
- Santhakumar V, Bender R, Frotscher M, Ross ST, Hollrigel GS, Toth Z, Soltesz I (2000) Granule cell hyperexcitability in the early post-traumatic rat dentate gyrus: the ‘irritable mossy cell’ hypothesis. *J Physiol* 524(Pt 1):117–134
- Santhakumar V, Aradi I, Soltesz I (2005) Role of mossy fiber sprouting and mossy cell loss in hyperexcitability: a network model of the dentate gyrus incorporating cell types and axonal topography. *J Neurophysiol* 93:437–453
- Scharfman HE (1995) Electrophysiological evidence that dentate hilar mossy cells are excitatory and innervate both granule cells and interneurons. *J Neurophysiol* 74:179–194
- Scharfman HE, Kunkel DD, Schwartkroin PA (1990) Synaptic connections of dentate granule cells and hilar neurons: results of paired intracellular recordings and intracellular horseradish peroxidase injections. *Neuroscience* 37:693–707
- Scorcioni R, Polavaram S, Ascoli GA (2008) L-measure: a web-accessible tool for the analysis, comparison and search of digital reconstructions of neuronal morphologies. *Nat Protoc* 3:866–876
- Seress L, Pokorny J (1978) Structure of the granular layer of the rat dentate gyrus. A light microscopic and Golgi study. *J Anat* 133:181–195
- Seress L, Pokorny J (1981) Structure of the granular layer of the rat dentate gyrus: a light microscopic and Golgi study. *J Anat* 133:181–195
- Seress L, Ribak CE (1983) GABAergic cells in the dentate gyrus appear to be local circuit and projection neurons. *Exp Brain Res* 50:173–182
- Sík A, Penttonen M, Buzsáki G (1997) Interneurons in the hippocampal dentate gyrus: an in vivo intracellular study. *Eur J Neurosci* 9:573–588
- Sloviter RS, Zappone CA, Harvey BD, Bumanglag AV, Bender RA, Frotscher M (2003) ‘Dormant basket cell’ hypothesis revisited: relative vulnerabilities of dentate gyrus mossy cells and inhibitory interneurons after hippocampal status epilepticus in the rat. *J Comp Neurol* 459:44–76
- Solstad T, Moser EI, Einevoll GT (2006) From grid cells to place cells: a mathematical model. *Hippocampus* 16:1026–1031. <https://doi.org/10.1002/hipo.20244>

- Soriano E, Frotscher M (1989) A GABAergic axo-axonic cell in the fascia dentata controls the main excitatory hippocampal pathway. *Brain Res* 503:170–174
- Soriano E, Frotscher M (1994) Mossy cells of the rat fascia dentate are glutamate-immunoreactive. *Hippocampus* 4:65–69
- Spruston N, Johnston D (1992) Perforated patch-clamp analysis of the passive membrane properties of three classes of hippocampal neurons. *J Neurophysiol* 67:508–529. <https://doi.org/10.1152/jn.1992.67.3.508>
- Squire LR (1986) Mechanisms of memory. *Science* 232:1612–1619
- Swanson LW, Wyss JM, Cowan WM (1978) An autoradiographic study of the organization of intrahippocampal association pathways in the rat. *J Comp Neurol* 181:681–716
- Tamamaki N, Nojyo Y (1993) Projection of the entorhinal layer II neurons in the rat as revealed by intracellular pressure-injection of neurobiotin. *Hippocampus* 3:471–480
- Treves A, Rolls ET (1994) Computational analysis of the role of the hippocampus in memory. *Hippocampus* 4:374–391
- Vida I (2010) Morphology of hippocampal neurons. In: Cutsuridis V, Graham BP, Cobb S, Vida I (eds) *Hippocampal microcircuits*. Springer, New York, pp 27–67
- Warman EN, Durand DM, Yuen GLF (1994) Reconstruction of hippocampal CA1 pyramidal cell electrophysiology by computer simulation. *J Neurosci* 14:2033–2045
- Wenzel HJ, Buckmaster PS, Anderson NL, Wenzel ME, Schwartzkroin PA (1997) Ultrastructural localization of neurotransmitter immunoreactivity in mossy cell axons and their synaptic targets in the rat dentate gyrus. *Hippocampus* 7:559–570
- Witter MP (2007) The perforant path: projections from the entorhinal cortex to the dentate gyrus. *Prog Brain Res* 163:43–61
- Yeckel MF, Berger TW (1990) Feedforward excitation of the hippocampus by entorhinal afferents: redefinition of the role of the trisynaptic pathway. *Proc Natl Acad Sci USA* 87:5832–5836
- Yeckel MF, Berger TW (1995) Monosynaptic excitation of CA1 hippocampal pyramidal neurons by afferents from the entorhinal cortex. *Hippocampus* 5:108–114
- Yu GJ, Song D, Berger TW (2014) Implementation of the excitatory entorhinal-dentate-CA3 topography in a large-scale computational model of the rat hippocampus. In: EMBC, 2014: 36th annual international conference of the IEEE Engineering in Medicine and Biology Society, Chicago. IEEE, pp 6581–6584
- Yu GJ, Hendrickson PJ, Song D, Berger TW (2015) Topography-dependent spatio-temporal correlations in the entorhinal-dentate-CA3 circuit in a large-scale computational model of the rat hippocampus. In: EMBC, 2015: 37th annual international conference of the IEEE Engineering in Medicine and Biology Society, Milan. IEEE, pp 3965–3968
- Yu GJ, Song D, Berger TW (2016). Place field detection using grid-based clustering in a large-scale computational model of the rat dentate gyrus. In: EMBC, 2016: 38th annual international conference of the IEEE Engineering in Medicine and Biology Society, Orlando. IEEE, pp 1405–1408
- Yuen GLF, Durand DM (1991) Reconstruction of hippocampal granule cell electrophysiology by computer simulation. *Neuroscience* 41:411–423
- Zimmer J (1971) Ipsilateral afferents to the commissural zone of the fascia dentata, demonstrated in decommissurated rats by silver impregnation. *J Comp Neurol* 142:393–416
- Zipp F, Nitsch R, Soriano E, Frotscher M (1989) Entorhinal fibers form synaptic contacts on parvalbumin-immunoreactive neurons in the rat fascia dentata. *Brain Res* 495:161–166